

# Seasonal Forecasts of the Exceptional Northern Hemisphere Winter of 2020

Simon Haydn Lee<sup>1,1</sup>, Zachary Duane Lawrence<sup>2,2</sup>, Amy Hawes Butler<sup>2,2</sup>, and Alexey Yurievich Karpechko<sup>3,3</sup>

<sup>1</sup>University of Reading

<sup>2</sup>CIRES/NOAA

<sup>3</sup>Finnish Meteorological Institute

November 30, 2022

## Abstract

The winter of 2019-20 was dominated by an extremely strong stratospheric polar vortex and positive tropospheric Arctic Oscillation (AO). Here, we analyze forecasts from 6 different prediction systems contributing to the C3S seasonal forecast database. Most performed very strongly, with consistently high skill for January-March 2020 from forecasts launched through October–December 2019. Although the magnitude of the anomalies was underestimated, the performance of most prediction systems was extremely high for a positive AO winter relative to the common hindcast climate. Ensemble members which better predicted the extremely strong stratospheric vortex better predicted the extreme tropospheric state. We find a significant relationship between forecasts of the anomalous mid-latitude tropospheric wave pattern in early winter, which destructively interfered with the climatological stationary waves, and the strength of the stratospheric vortex later in the winter. Our results demonstrate a strong interdependence between the accuracy of stratospheric vortex and AO forecasts.

# Seasonal Forecasts of the Exceptional Northern Hemisphere Winter of 2020

Simon H. Lee<sup>1</sup>, Zachary D. Lawrence<sup>2,3</sup>, Amy H. Butler<sup>4</sup>, and Alexey Y. Karpechko<sup>5</sup>

<sup>1</sup>Department of Meteorology, University of Reading, Reading, UK

<sup>2</sup>Cooperative Institute for Research in Environmental Sciences (CIRES), University of Colorado, Boulder, Colorado, USA

<sup>3</sup>NOAA Physical Sciences Laboratory (PSL), Boulder, Colorado, USA

<sup>4</sup>NOAA Chemical Sciences Laboratory (CSL), Boulder, Colorado, USA

<sup>5</sup>Finnish Meteorological Institute, Helsinki, Finland

## Key Points:

- Forecasts from 6 seasonal prediction systems consistently predicted the large-scale winter patterns with unusually high accuracy.
- Ensemble members which better predicted the extreme stratospheric state also better predicted the extreme tropospheric state.
- Accurate prediction of the mid-latitude tropospheric wave pattern was associated with more accurate stratospheric forecasts.

---

Corresponding author: Simon H. Lee, [s.h.lee@pgr.reading.ac.uk](mailto:s.h.lee@pgr.reading.ac.uk)

## Abstract

The winter of 2019-20 was dominated by an extremely strong stratospheric polar vortex and positive tropospheric Arctic Oscillation (AO). Here, we analyze forecasts from 6 different prediction systems contributing to the C3S seasonal forecast database. Most performed very strongly, with consistently high skill for January–March 2020 from forecasts launched through October–December 2019. Although the magnitude of the anomalies was underestimated, the performance of most prediction systems was extremely high for a positive AO winter relative to the common hindcast climate. Ensemble members which better predicted the extremely strong stratospheric vortex better predicted the extreme tropospheric state. We find a significant relationship between forecasts of the anomalous mid-latitude tropospheric wave pattern in early winter, which destructively interfered with the climatological stationary waves, and the strength of the stratospheric vortex later in the winter. Our results demonstrate a strong interdependence between the accuracy of stratospheric vortex and AO forecasts.

## Plain Language Summary

Westerly winds during the winter of 2019-20 were unusually strong and long lasting through a deep layer of the atmosphere. We investigate how well this was predicted months ahead of time. We find that seasonal weather forecast systems predicted the winter pattern very well, especially when compared with previous winters. Forecasts which better predicted the strength of the winds higher in the atmosphere did better overall. We find that there was a link between predictions of the weather patterns lower down in the atmosphere and how they suppressed large-scale atmospheric waves in the mid-latitudes, which likely helped the winds remain stronger higher up.

## 1 Introduction

The Northern Hemisphere (NH) winter of 2019-20, particularly January–March (JFM) 2020, was characterized by a strong and persistent positive phase of the Arctic Oscillation (AO) (Hardiman et al., 2020; Lawrence et al., submitted) – the leading mode of extratropical tropospheric wintertime variability, analogous to the surface Northern Annular Mode (NAM) (e.g. Thompson & Wallace, 1998, 2001; Black & McDaniel, 2004) and closely-related to the North Atlantic Oscillation (NAO) (Feldstein & Franzke, 2006). The magnitude and persistence of this pattern, associated with strengthened and poleward-shifted extratropical storm tracks, led to unusually warm conditions across NH mid-latitudes, as well as hydrometeorological extremes associated with the shifted storm tracks. For example, while the United Kingdom experienced its wettest February since at least 1862, Spain experienced its driest February in at least 56 years (NOAA, 2020). Coupled to the strongly positive tropospheric NAM was an extremely strong stratospheric polar vortex (SPV) (Lawrence et al., submitted); significant disturbances to the SPV, so-called sudden stratospheric warmings (SSWs) (e.g. Charlton & Polvani, 2007; Butler et al., 2015), were entirely absent during their climatological peak of January–March. The record-cold temperatures within the undisturbed SPV led to unprecedented ozone loss over the Arctic during spring 2020 (Manney et al., 2020; Wohltmann et al., 2020). Thus, the winter of 2020 represents a vertically-deep, extreme climatic state, which offers a rare opportunity to test the performance of operational seasonal forecast models in predicting such an extreme.

Seasonal forecast models have demonstrated significant skill in predicting large-scale wintertime climate modes such as the NAO/AO (Scaife et al., 2014), though with significant year-to-year variability. A component of this predictability may arise from the SPV state at the start of the winter (Nie et al., 2019) and accurate predictions of the likelihood of extreme SPV states during the winter (both strong vortex events and SSWs) due to their relatively long persistence (Scaife et al., 2016). Additional influences on the

seasonal-mean NAO/AO and SPV include: tropical sea surface temperatures (SSTs) and precipitation, including the El Niño-Southern Oscillation (ENSO) and Indian Ocean SSTs (Fletcher & Cassou, 2015; Hall et al., 2017; Baker et al., 2019; Trascasa-Castro et al., 2019; Domeisen et al., 2019), Atlantic SSTs (Rodwell & Folland, 2002; W. Wang et al., 2004; Hall et al., 2017) and North Pacific SSTs (Hurwitz et al., 2012). These can interact directly through forcing tropospheric Rossby wave trains, or indirectly by influencing the strength of the SPV (e.g. Ineson & Scaife, 2009) through modulation of vertically propagating wave activity. Some of the aforementioned drivers have been used with some success in statistical forecasts (e.g. Folland et al., 2012; Riddle et al., 2013; Hall et al., 2017; L. Wang et al., 2017) to elucidate sources of predictability in dynamical models.

In this letter, we analyze how well the extreme large-scale circulation patterns present during winter (JFM) 2020 were predicted by seasonal forecasts issued during late 2019 from different prediction systems. We assess whether forecasts that more accurately captured the SPV strength better captured the strength of the positive tropospheric AO and overall NH pattern, given their close statistical and dynamical link. We also investigate possible drivers of the extreme winter pattern.

## 2 Data and Methods

We analyze data from 6 prediction systems that contribute to the Copernicus Climate Change Service (C3S) seasonal forecast database – namely, from the United Kingdom Met Office (UKMO), the European Centre for Medium-range Weather Forecasts (ECMWF), Météo-France, Deutsche Wetterdienst (DWD), the National Centers for Environmental Prediction (NCEP), and the Euro-Mediterranean Center on Climate Change (Centro euro-Mediterraneo sui Cambiamenti Climatici; CMCC). Data are provided at 1° latitude-longitude resolution. As stratospheric-level data from NCEP are not currently available from C3S, it is not included in the multi-model comparison for that part of the analysis. Table S1 provides details of the individual model systems used. All model anomalies are expressed with respect to the common hindcast initialization period 1993–2016. Additionally, the multi-model mean (MMM) is calculated as the average of the ensemble means of the 6 models. Verification is performed with the ECMWF ERA5 reanalysis at 1.0° resolution (Hersbach et al., 2020), with anomalies computed with respect to the monthly December 1993–March 2017 climatology.

The anomaly correlation coefficient (ACC) (e.g. Wilks, 2019) over a domain between a forecast anomaly  $f$  at each grid point  $i,j$  and corresponding observation  $o$ , weighted by cosine-latitude  $w$ , is calculated using:

$$ACC = \frac{cov(f, o; w)}{\sqrt{cov(f, f; w)cov(o, o; w)}} \quad (1)$$

where the weighted covariance is calculated as:

$$cov(f, o; w) = \frac{\sum_i \sum_j w_{i,j} (f_{i,j} - \bar{f}_w)(o_{i,j} - \bar{o}_w)}{\sum_i \sum_j w_{i,j}} \quad (2)$$

where the overbar indicates the weighted average across the domain.

The AO index is computed as the leading empirical orthogonal function (EOF) of JFM-averaged mean sea level pressure (MSLP) anomalies poleward of 20°N (e.g. Thompson & Wallace, 1998) over the period December 1993–March 2017 in ERA5, which explains 27% of the total variance. Anomalies are weighted by the square-root of cosine-latitude to give equal area weighting. In the seasonal forecasts and the ERA5 verification, the forecast AO index is computed as the projection of the ERA5 EOF onto the

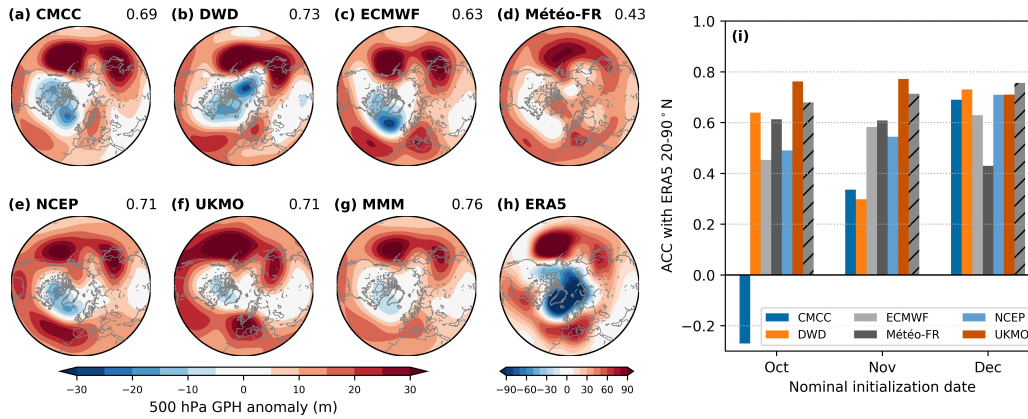


**Figure 1.** (a–f) Average January–March 2020 ensemble-mean 500 hPa geopotential height (Z500 GPH) anomalies, poleward of 20°N, from 6 seasonal prediction systems nominally initialized on 1 December 2019. Anomalies are expressed with respect to the 1993–2016 hindcast climatology for each prediction system. (g) Multi-model mean (MMM) of a–f. (h) As in panels a–g but for ERA5 reanalysis. Due to the larger anomaly magnitudes in ERA5, a separate color scale is used. The number in the top-right of panels a–g indicates the anomaly correlation coefficient (ACC) with ERA5. (i) ACC between ensemble-mean JFM-mean Z500 anomalies poleward of 20°N and ERA5, for nominal initialization dates of October, November, and December 2019. The MMM is shown as a hatched bar.

111 forecast/reanalysis MSLP anomalies, and is scaled to have unit standard deviation (across  
 112 all ensemble members) over the hindcast period in each model and ERA5.

### 113 3 Tropospheric Forecasts

114 We first assess the skill of the seasonal forecasts by considering predictions of the  
 115 extratropical mid-tropospheric flow. Aside from regional subtleties, Figure 1 shows that  
 116 all systems predicted strikingly similar patterns on the hemispheric scale – both with each  
 117 other and with ERA5, though with characteristically low signal amplitude (e.g. Scaife  
 118 et al., 2014). The similarity with ERA5 is reflected in the high ACCs, which exceed 0.6  
 119 for all but Météo-France (0.43) and otherwise range from 0.63 (ECMWF) to 0.73 (DWD)  
 120 for the individual prediction systems, while the MMM performed the best (0.76). There  
 121 are several key features of the observed wintertime state (Fig. 1h): (i) a strongly posi-  
 122 tive NAO pattern, with an enhanced poleward height gradient in the Atlantic sector,  
 123 (ii) a large anomalous ridge in the northeast Pacific, (iii) a secondary ridge anomaly in  
 124 eastern Asia and the northwest Pacific. All systems predicted the Pacific ridge anoma-  
 125 lies, though in Météo-France only 1 broad anomalous ridge was predicted. All but Météo-  
 126 France predicted the enhanced Iceland low and Azores high characteristic of the posi-  
 127 tive NAO.

128 Another feature of the seasonal forecasts of winter 2020 was their general consis-  
 129 tency in predicting a similar pattern across different initializations. Equivalent maps as  
 130 Figure 1 but for October and November forecasts are provided in the supporting infor-  
 131 mation (Figure S1–S2). For brevity, we show the ACCs for these forecasts in Figure 1i.  
 132 The highest-performing forecasts were the October and November forecasts from UKMO,  
 133 which had ACCs of 0.76 and 0.77 respectively. The MMM performed very strongly across  
 134 the initialization dates despite considerable inter-model differences, with an ACC of 0.68-  
 135 0.76, only exceeded by the forecasts from UKMO in October and November. The lowest-

136 performing forecasts were the October initialization from CMCC (-0.27), and both Oc-  
 137 tober and November initializations from CMCC (0.34) and DWD (0.30). In these cases,  
 138 a notable missing feature was the anomalous ridge in the northeast Pacific.

139 The ACC skill of the forecasts for winter 2020 was unusually high with respect to  
 140 the common hindcast period. Figure 2 shows the JFM ACCs for hindcasts nominally  
 141 initialized on 1 December 1993–2016, alongside the ACC for the 2020 forecast. As the  
 142 operational forecast ensemble sizes are larger than the hindcast ensembles (c.f. Table S1),  
 143 we also show a 95% confidence interval around the 2020 forecast obtained by randomly  
 144 sub-sampling the operational forecast ensemble to the size of the hindcast ensemble 10,000  
 145 times. When accounting for this uncertainty, the performance of all systems except Météo-  
 146 France exceeded more than half of the hindcast years; without the uncertainty estimate  
 147 the skill of the full ensemble exceeded more years. Only JFM 1998 and 2010 lie within  
 148 the confidence interval for CMCC, the lowest resolution model; unlike 2020, both were  
 149 significant El Niño years, and neither were positive AO/NAO winters (2010 in fact was  
 150 dominated by an extremely *negative* AO/NAO). We also note that the mean of the re-  
 151 sampled ACCs was systematically smaller than the ACCs of the full ensemble (not shown),  
 152 consistent with the need for large ensemble sizes to produce skillful forecasts (Scaife et  
 153 al., 2014).

154 As suggested by Figure 1, all but Météo-France predicted a positive AO for JFM  
 155 2020 (Figure 3a). However, the ensemble-mean forecasts were about  $0.5 \sigma$ , much less than  
 156 the observed value of  $2.4 \sigma$ ; only the ensemble spread of DWD and NCEP contained the  
 157 true value. The lack of an ensemble-mean signal for a positive AO in Météo-France is  
 158 consistent with its lower hemispheric ACC (c.f. Fig. 1d). The highest observed JFM-  
 159 mean AO index during 1994–2017 is  $1.7 \sigma$  in JFM 2015; thus, there is not a similar year  
 160 within the common hindcast period with which we can compare 2020. The upper-tail  
 161 of the UKMO predictions lay outside the model hindcast climatology, and was thus the  
 162 only prediction system with ensemble members predicting a record-positive AO. Addi-  
 163 tionally, Figure 3b shows that, in contrast with ERA5, the ensemble-mean AO index was  
 164 not a record for any of the models with respect to their hindcasts.

#### 165 4 Stratospheric Polar Vortex Forecasts

166 We next consider predictions of the seasonal-mean SPV, defined as the JFM-averaged  
 167 zonal-mean zonal wind at 10 hPa and  $60^\circ\text{N}$  (following e.g. Charlton and Polvani (2007)).  
 168 Boxplots of the ensemble distributions from the December 2019 initializations, along with  
 169 the corresponding hindcast distribution, are shown in Figure 4a. The verifying anomaly  
 170 according to ERA5 was  $20.0 \text{ m s}^{-1}$ ; this is only exceeded by JFM 1997 ( $23.2 \text{ m s}^{-1}$ ) in  
 171 the hindcast period. The ensemble-mean of all systems shown here predicted a stronger-  
 172 than-average SPV with respect to their own climatological mean state (although the de-  
 173 parture was very small for Météo-France), with the greatest departure predicted by DWD  
 174 ( $7.2 \text{ m s}^{-1}$ ). Similarly, the true anomaly magnitude lay within the ensemble spread of  
 175 all except Météo-France. Fig. 4b shows that the ensemble-mean forecasts for JFM 2020  
 176 from both CMCC and DWD exceeded any equivalent in their hindcast periods indicat-  
 177 ing there was an exceptional ensemble-mean signal from these prediction systems for a  
 178 strong seasonal-mean SPV. This is in contrast to the ensemble-mean AO forecasts, which  
 179 were not a record with respect to the hindcast period for any prediction system.

180 We further assess the relationship between the accuracy of SPV forecasts with the  
 181 accuracy of the AO to assess whether accurate predictions of the anomalous SPV strength  
 182 were associated with more accurate predictions of the large-scale tropospheric state. Fig-  
 183 ure 4c shows that, in all but Météo-France, there was a significant positive correlation  
 184 between the AO error and the SPV error; ensemble members with a stronger SPV tended  
 185 to have a more positive AO. This linear relationship was strongest in ECMWF ( $r = 0.68$ ),  
 186 DWD ( $r = 0.65$ ) and UKMO ( $r = 0.64$ ). The lack of a significant correlation in Météo-

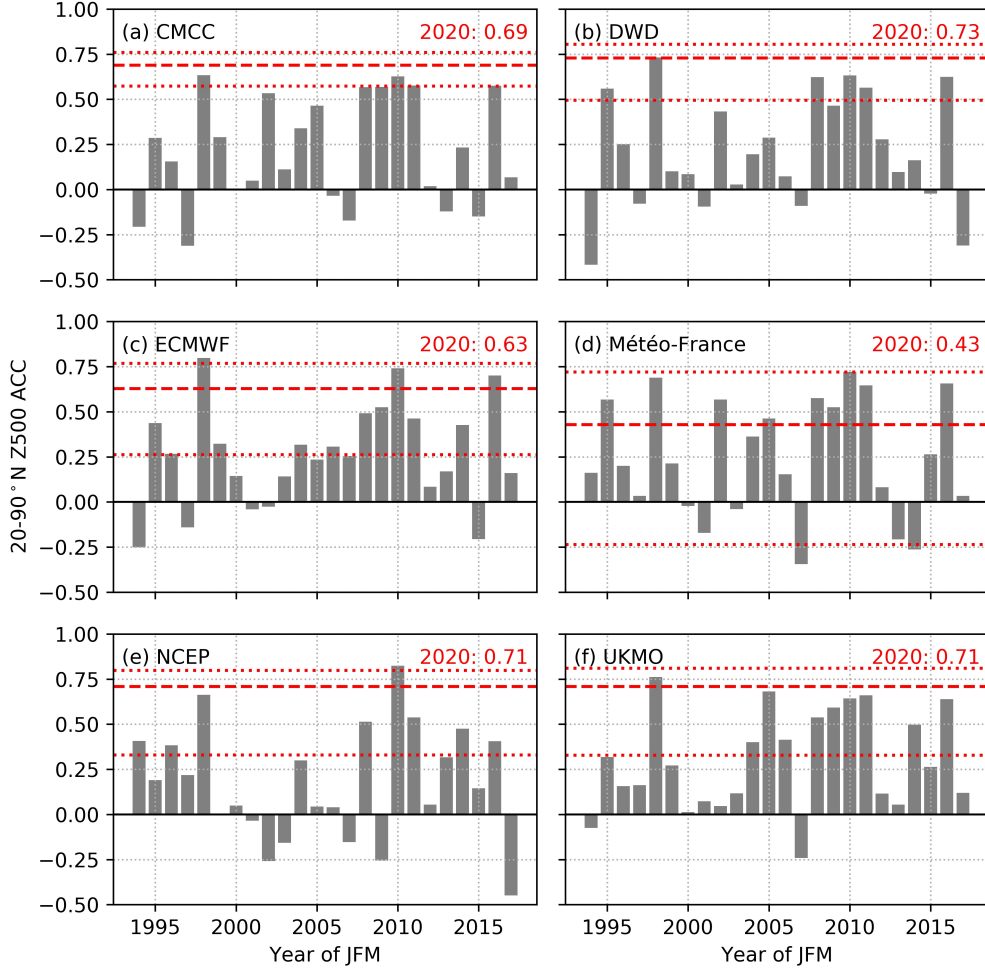


**Figure 2.** ACCs (gray bars) between ensemble-mean JFM-mean Z500 poleward of 20°N and ERA5 for nominal 1 December hindcasts in the common period 1993–2016. Dashed red lines are the respective ACCs from the December 2019 forecast; dotted red lines indicate the 95% confidence interval obtained by re-sampling the forecast ensemble to the size of the hindcast ensemble 10,000 times (without replacement).

187 France is interesting given it predicted both the weakest SPV and least-positive AO. Thus,  
 188 the linear relationship between the AO and SPV was only evident in the prediction sys-  
 189 tems which indicated an increased likelihood of a stronger SPV (c.f. Figure 5a).

190 As seasonal-mean statistics may mask sub-seasonal variability, we also compute the  
 191 probability of strong or weak SPV events using daily data from the December forecasts,  
 192 and compare with the climatological likelihood. The threshold for a strong/weak vor-  
 193 tex is set at the 80th/20th percentiles of the daily hindcast zonal wind distribution for  
 194 JFM 1994–2017 in each model. We apply a relatively long persistence criterion of 5 days  
 195 to capture anomalous SPV states with potentially higher seasonal impact. Figure 5a shows  
 196 that, for all but Météo-France, the probability of a strong vortex in JFM 2020 was sig-  
 197 nificantly elevated with respect to the mean over the JFM 1994–2017 hindcast climate.  
 198 Correspondingly, the probability of a weak vortex was reduced (Fig. 5b). Forecasts from  
 199 DWD indicated a significantly greater probability of a strong vortex than any winter in  
 200 the hindcasts. CMCC nominally indicated a lower chance of a weak vortex than any win-

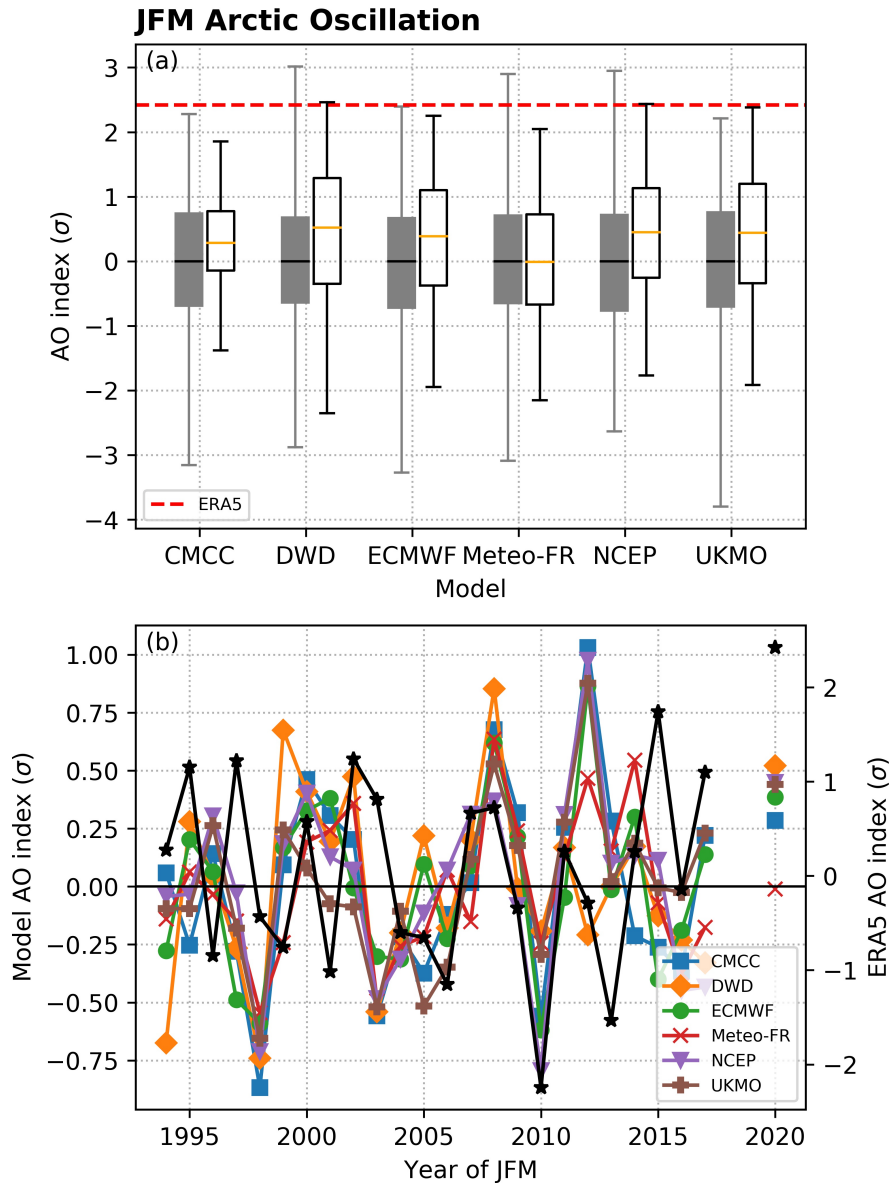


**Figure 3.** (a) Forecasts of the average JFM 2020 Arctic Oscillation (non-filled boxes), for 6 seasonal prediction systems nominally initialized on 1 December 2019. Solid gray boxes show the corresponding hindcast distribution for JFM 1994–2017. Horizontal lines indicate the mean. Whiskers extend to the extreme values. The observed anomaly from ERA5 ( $2.4 \sigma$ ) is shown with a horizontal red line. Units are standard deviations of the corresponding hindcast/reanalysis climatology. (b) Ensemble-mean AO hindcasts for JFM 1994–2017 (left-hand ordinate) and ERA5 (right-hand ordinate). The ensemble-mean forecasts and ERA5 for JFM 2020 are also shown.

201 ter in the hindcast period, but the effect of the different ensemble sizes means this dif-  
 202 ference was not significant. These results are consistent with Figure 4b. Moreover, the  
 203 absence of a significant departure in the likelihood of a strong or weak vortex in Météo-  
 204 France is in agreement with its poorer ACC and the absence of a signal for a strongly  
 205 positive AO.

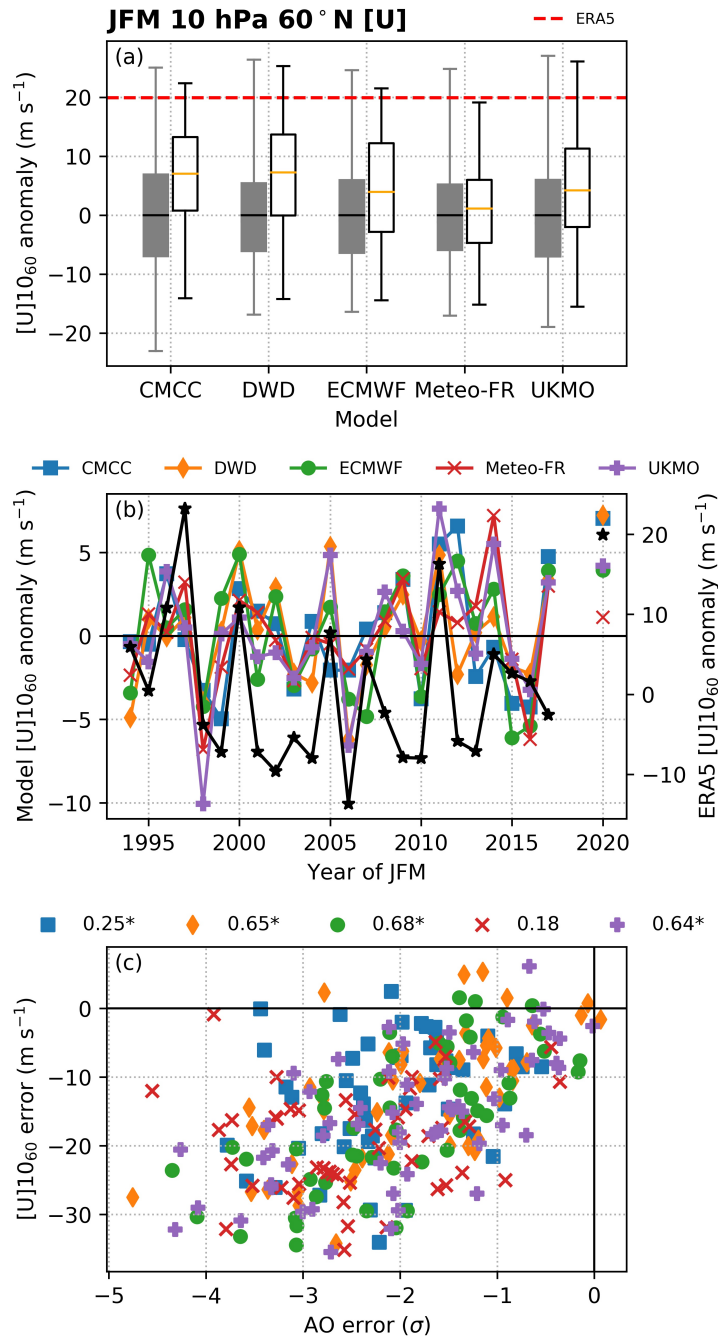


**Figure 4.** (a, b) As in Figure 3 but for the zonal-mean zonal wind anomaly at 10 hPa and 60°N, excluding forecasts from NCEP. (c) Scatter plot of individual ensemble member forecasts of the JFM 2020 AO and  $[U]_{10_{60}}$ , as departures from the ERA5 value. Correlation values are shown, and an asterisk indicates the correlation is significant at the 95% confidence level after 10,000 bootstrap re-samples with replacement.

206

## 5 Linking Tropospheric and Stratospheric Forecasts

207

In this final section we seek to link features in the tropospheric forecasts with those in the stratosphere, using lagged linear regression between different variables across all

208

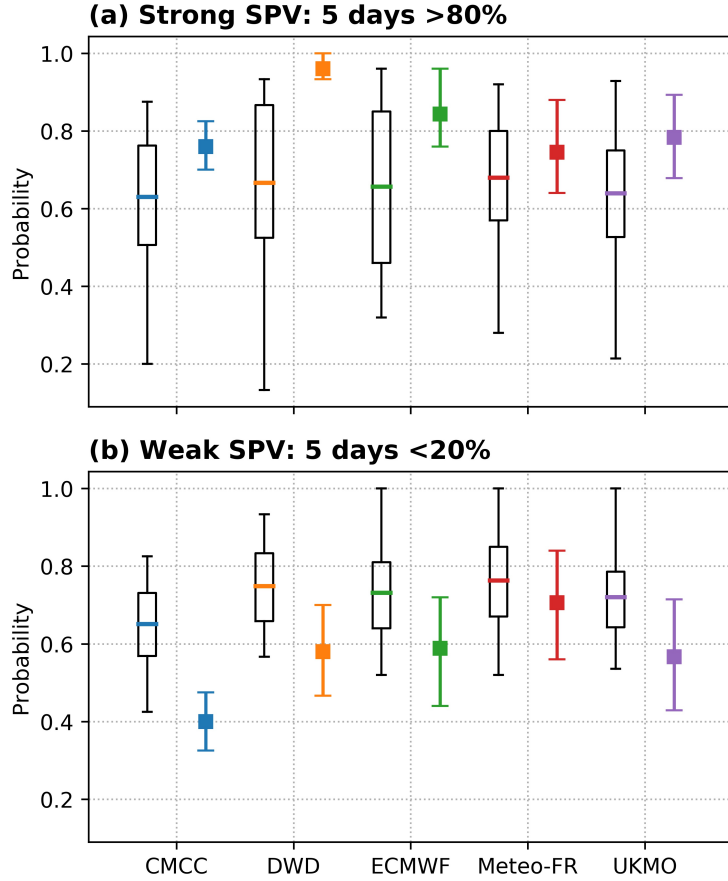


**Figure 5.** Probability of (a) strong and (b) weak vortex events for JFM from nominal 1 December initializations, using thresholds based on the hindcast climate in each model. Boxplots indicate the hindcast distribution, with the mean indicated by the horizontal line. Squares indicate the probability for JFM 2020. Error bars are a 95% uncertainty estimate by re-sampling the operational ensemble to the size of the hindcast ensemble 10,000 times (without replacement).

209 members of a multi-model ensemble (also known as “ensemble sensitivity analysis”, e.g.  
 210 Dacre and Gray (2013)). First, the individual ensemble mean is subtracted from each  
 211 ensemble member to produce a perturbation anomaly, and then scaled by the ensemble  
 212 standard deviation, before then forming the multi-model ensemble. The resultant lin-  
 213 ear regression coefficients are thus in units of standard deviation of the “response” (lead-  
 214 ing) variable per standard deviation in the “precursor” variable.

215 The relationship between 500 hPa geopotential height (Z500) anomalies in January  
 216 and the February–March SPV strength is shown in Figure 6a. The hemispheric-wide pat-  
 217 tern of the regression coefficients is similar to both the ERA5 verification and the fore-  
 218 casts with the highest ACCs in Figure 1, exhibiting significant destructive interference  
 219 with the climatological-mean eddy height field. The destructive interference that was re-  
 220 lated to forecasts of a stronger SPV was particularly strong in the North Pacific (destructively  
 221 interfering with the climatological Aleutian low), western North America, and north-  
 222 eastern Scandinavia and the Ural mountains region. The absence of blocking in the Ural  
 223 region is in contrast to the SSW precursor patterns (e.g. Karpechko et al., 2018; Lee et  
 224 al., 2019; Peings, 2019). Similar, albeit weaker, results are found when using Z500 in De-  
 225 cember and JFM SPV forecasts (not shown). These results are consistent with Lawrence

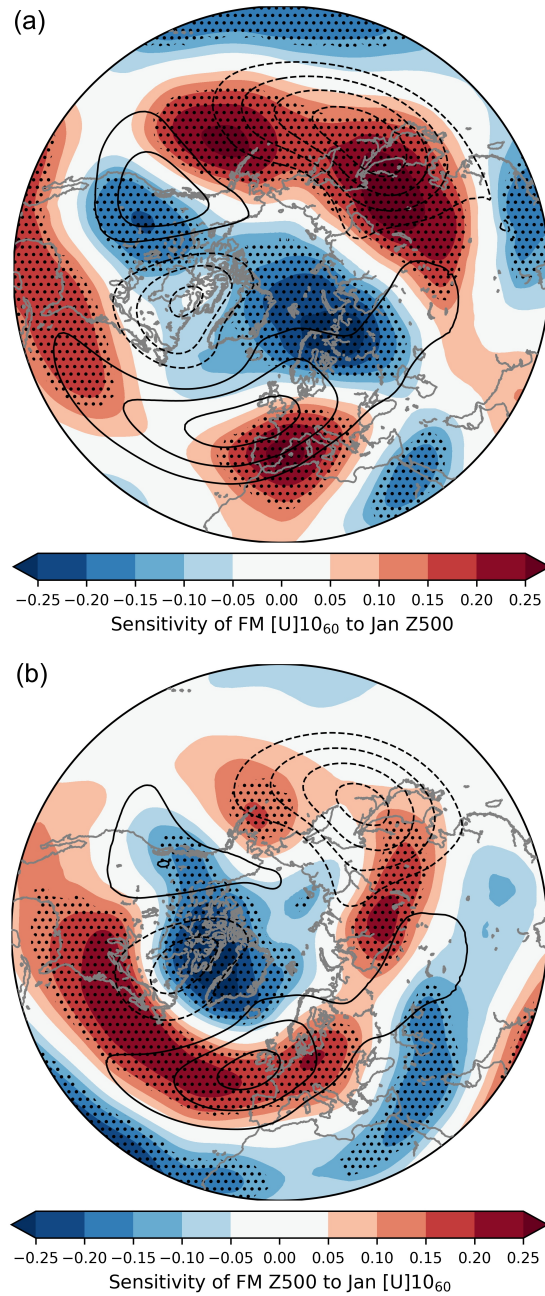


**Figure 6.** Ensemble sensitivity, across all ensemble members (except NCEP) from the 1 December 2019 initialization, between forecasts of (a) January Z500 and February–March (FM) [U]10<sub>60</sub> and (b) January [U]10<sub>60</sub> and FM Z500. Units are standardized departures from the ensemble mean. The corresponding 1994–2017 average eddy height field from ERA5 are shown in contours (every 50 m from -200 to 200 m, excluding 0). Stippling indicates significance at the 95% confidence level after 10,000 bootstrap re-samples (with replacement).

226  
227

et al. (submitted) who found that low vertically-propagating tropospheric wave activity was present during the winter.

228 We also show in Figure 6b that ensemble members which predicted a stronger SPV  
229 in January tended to predict a tropospheric anomaly pattern consistent with the pos-  
230 itive AO/NAO during February–March, in agreement with Figure 4c. The strongest sensi-  
231 tivity of the FM Z500 anomalies to January SPV strength is over the North Atlantic,  
232 where the downward influence of the stratosphere on the troposphere has been found to  
233 dominate (Hitchcock & Simpson, 2014). The results in Figure 6 cannot be used to infer  
234 causality behind the anomalies in Figure 1, but do suggest that the spread in sea-  
235 sonal forecasts depended on how well the prediction systems captured the two-way cou-  
236 pling process. In particular, these results suggest that both the accurate prediction of  
237 certain mid-latitude tropospheric anomalies in early mid-winter was important in the  
238 subsequent prediction of the extremely strong SPV (through suppression of the mean  
239 wave field), and that a stronger SPV in early-mid winter was associated with a more pos-  
240 itive AO later in the winter, likely through downward coupling of persistent stratospheric  
241 anomalies.

## 242 6 Summary

243 In this letter, we have analyzed the performance of forecasts for the exceptional win-  
244 ter of 2020 from 6 seasonal prediction systems which contribute to the C3S seasonal fore-  
245 cast database. Our results show that the performance of the majority of the models in  
246 predicting the extratropical anomaly pattern was among the highest in the common hind-  
247 cast period, particularly for a positive AO winter in the absence of a major ENSO event.  
248 We also find that, despite large differences between individual models, the multi-model  
249 mean had the most consistently high skill – supporting the usefulness of a multi-model  
250 approach. Otherwise, the most consistently skillful forecasts were from UKMO. Of the  
251 forecasts from December 2019, only Météo-France did not predict the positive AO or strong  
252 SPV, and accordingly had the lowest extratropical skill (though earlier initializations per-  
253 formed better, c.f. Figure S1-S2). Although the forecasts systematically underestimated  
254 the extreme magnitude of the anomalous AO, the ensemble-mean SPV forecasts from  
255 CMCC and DWD exceeded any winter in their hindcasts, indicating the relatively ex-  
256 treme state was predicted by these models.

257 We further find that ensemble members that predicted a stronger SPV also pre-  
258 dicted a stronger AO, suggesting that the prediction of the strong SPV also played a role  
259 in accurate predictions of the large-scale surface circulation pattern, consistent with Scaife  
260 et al. (2016). For all systems except Météo-France, there were significant increases in the  
261 probability of a strong SPV and a decreased probability of a weak SPV/SSW – though  
262 these were generally not exceptional with respect to the hindcast period. Nevertheless,  
263 this shows that these seasonal forecasts correctly indicated the shift in the likelihood of  
264 these sub-seasonal phenomena.

265 An ensemble sensitivity analysis showed that ensemble members that predicted greater  
266 destructive interference with the tropospheric stationary waves in early winter predicted  
267 a stronger SPV later in the winter, in a pattern concordant with the overall anomaly field  
268 during winter 2020. This result suggests a two-way relationship between the troposphere  
269 and stratosphere during the winter. Modeling experiments, following those of Hardiman  
270 et al. (2020) who tied NAO predictability to the Indian Ocean Dipole event in late 2019,  
271 will likely be required to fully elucidate the cause of this tropospheric predictability, and  
272 ascertain why it was better captured by some prediction systems at much longer lead-  
273 times than others.

## 274 Acknowledgments

275 SHL acknowledges funding by the Natural Environment Research Council (NERC) via  
276 the SCENARIO Doctoral Training Partnership (NE/L002566/1). ZDL acknowledges sup-  
277 port from Federally Appropriated Funds. AYK acknowledges funding from the Academy

278 of Finland (project number 286298). The C3S seasonal forecast database and ERA5 re-  
279 analysis are available online through the Copernicus Climate Data Store at [https://](https://cds.climate.copernicus.eu/)  
280 [cds.climate.copernicus.eu/](https://cds.climate.copernicus.eu/). Operational C3S forecast products are available at [https://](https://climate.copernicus.eu/charts/c3s_seasonal/)  
281 [climate.copernicus.eu/charts/c3s\\_seasonal/](https://climate.copernicus.eu/charts/c3s_seasonal/). We thank two anonymous review-  
282 ers for their helpful comments which improved the paper.

283 **References**

- 284 Baker, H. S., Woollings, T., Forest, C. E., & Allen, M. R. (2019). The linear sen-  
 285 sitivity of the north atlantic oscillation and eddy-driven jet to ssts. *Journal of*  
 286 *Climate*, *32*(19), 6491–6511. doi: 10.1175/JCLI-D-19-0038.1
- 287 Black, R. X., & McDaniel, B. A. (2004). Diagnostic case studies of the northern  
 288 annular mode. *Journal of Climate*, *17*(20), 3990–4004. doi: 10.1175/1520  
 289 -0442(2004)017<3990:DCSOTN>2.0.CO;2
- 290 Butler, A. H., Seidel, D. J., Hardiman, S. C., Butchart, N., Birner, T., & Match, A.  
 291 (2015). Defining sudden stratospheric warmings. *Bulletin of the American*  
 292 *Meteorological Society*, *96*(11), 1913–1928. doi: 10.1175/BAMS-D-13-00173.1
- 293 Charlton, A. J., & Polvani, L. M. (2007). A new look at stratospheric sudden  
 294 warmings. part i: Climatology and modeling benchmarks. *Journal of Climate*,  
 295 *20*(3), 449–469. doi: 10.1175/JCLI3996.1
- 296 Dacre, H. F., & Gray, S. L. (2013). Quantifying the climatological relationship be-  
 297 tween extratropical cyclone intensity and atmospheric precursors. *Geophysical*  
 298 *Research Letters*, *40*(10), 2322–2327. doi: 10.1002/grl.50105
- 299 Domeisen, D. I., Garfinkel, C. I., & Butler, A. H. (2019). The teleconnection of el  
 300 niño southern oscillation to the stratosphere. *Reviews of Geophysics*, *57*(1), 5–  
 301 47. doi: 10.1029/2018RG000596
- 302 Feldstein, S. B., & Franzke, C. (2006). Are the north atlantic oscillation and the  
 303 northern annular mode distinguishable? *Journal of the Atmospheric Sciences*,  
 304 *63*(11), 2915–2930. doi: 10.1175/JAS3798.1
- 305 Fletcher, C. G., & Cassou, C. (2015). The dynamical influence of separate tele-  
 306 connections from the pacific and indian oceans on the northern annular mode.  
 307 *Journal of Climate*, *28*(20), 7985–8002. doi: 10.1175/JCLI-D-14-00839.1
- 308 Folland, C., Scaife, A., Lindesay, J., & Stephenson, D. (2012). How potentially  
 309 predictable is northern european winter climate a season ahead? *International*  
 310 *Journal of Climatology*, *32*(6), 801–818. doi: 10.1002/joc.2314
- 311 Hall, R. J., Scaife, A. A., Hanna, E., Jones, J. M., & Erdélyi, R. (2017). Simple  
 312 statistical probabilistic forecasts of the winter nao. *Weather and Forecasting*,  
 313 *32*(4), 1585–1601. doi: 10.1175/WAF-D-16-0124.1
- 314 Hardiman, S. C., Dunstone, N. J., Scaife, A. A., Smith, D. M., Knight, J. R.,  
 315 Davies, P., . . . Greatbatch, R. J. (2020). Predictability of european winter  
 316 2019/20: Indian ocean dipole impacts on the nao. *Atmospheric Science*  
 317 *Letters*, e1005. doi: 10.1002/asl.1005
- 318 Hersbach, H., Bell, B., Berrisford, P., Hirahara, S., Horányi, A., Muñoz-Sabater, J.,  
 319 . . . others (2020). The ERA5 global reanalysis. *Quarterly Journal of the Royal*  
 320 *Meteorological Society*. doi: 10.1002/qj.3803
- 321 Hitchcock, P., & Simpson, I. R. (2014). The downward influence of stratospheric  
 322 sudden warmings. *Journal of the Atmospheric Sciences*, *71*(10), 3856–3876.  
 323 doi: 10.1175/JAS-D-14-0012.1
- 324 Hurwitz, M. M., Newman, P., & Garfinkel, C. (2012). On the influence of north pa-  
 325 cific sea surface temperature on the arctic winter climate. *Journal of Geophys-  
 326 ical Research: Atmospheres*, *117*(D19). doi: 10.1029/2012JD017819
- 327 Ineson, S., & Scaife, A. (2009). The role of the stratosphere in the european climate  
 328 response to el niño. *Nature Geoscience*, *2*(1), 32–36. doi: 10.1038/ngeo381
- 329 Karpechko, A. Y., Charlton-Perez, A., Balmaseda, M., Tyrrell, N., & Vitart, F.  
 330 (2018). Predicting sudden stratospheric warming 2018 and its climate impacts  
 331 with a multimodel ensemble. *Geophysical Research Letters*, *45*(24), 13–538.  
 332 doi: 10.1029/2018GL081091
- 333 Lawrence, Z. D., Perlwitz, J., Butler, A. H., Manney, G. L., Newman, P. A., Lee,  
 334 S. H., & Nash, E. R. (submitted). The remarkably strong arctic strato-  
 335 spheric polar vortex of winter 2020: Links to record-breaking arctic oscilla-  
 336 tion and ozone loss. *Journal of Geophysical Research: Atmospheres*. doi:  
 337 10.1002/essoar.10503356.1

- 338 Lee, S. H., Charlton-Perez, A., Furtado, J., & Woolnough, S. (2019). Abrupt strato-  
 339 spheric vortex weakening associated with north atlantic anticyclonic wave  
 340 breaking. *Journal of Geophysical Research: Atmospheres*, *124*(15), 8563–8575.  
 341 doi: 10.1029/2019JD030940
- 342 Manney, G. L., Livesey, N. J., Santee, M. L., Froidevaux, L., Lambert, A., Lawrence,  
 343 Z., ... others (2020). Record-low arctic stratospheric ozone in 2020: Mls obser-  
 344 vations of chemical processes and comparisons with previous extreme winters.  
 345 *Geophysical Research Letters*. doi: 10.1029/2020GL089063
- 346 Nie, Y., Scaife, A. A., Ren, H.-L., Comer, R. E., Andrews, M. B., Davis, P., & Mar-  
 347 tin, N. (2019). Stratospheric initial conditions provide seasonal predictability  
 348 of the north atlantic and arctic oscillations. *Environmental Research Letters*,  
 349 *14*(3), 034006. doi: 10.1088/1748-9326/ab0385
- 350 NOAA. (2020). *National Centers for Environmental Information State of the Cli-*  
 351 *mate: Global Climate Report for February 2020*. Retrieved 2020-06-30, from  
 352 <https://www.ncdc.noaa.gov/sotc/global/202002>
- 353 Peings, Y. (2019). Ural blocking as a driver of early-winter stratospheric warm-  
 354 ings. *Geophysical Research Letters*, *46*(10), 5460–5468. doi: 10.1029/  
 355 2019GL082097
- 356 Riddle, E. E., Butler, A. H., Furtado, J. C., Cohen, J. L., & Kumar, A. (2013).  
 357 Cfsv2 ensemble prediction of the wintertime arctic oscillation. *Climate dynam-*  
 358 *ics*, *41*(3-4), 1099–1116. doi: 10.1007/s00382-013-1850-5
- 359 Rodwell, M., & Folland, C. (2002). Atlantic air–sea interaction and seasonal pre-  
 360 dictability. *Quarterly Journal of the Royal Meteorological Society*, *128*(583),  
 361 1413–1443. doi: 10.1002/qj.200212858302
- 362 Scaife, A., Arribas, A., Blockley, E., Brookshaw, A., Clark, R., Dunstone, N.,  
 363 ... others (2014). Skillful long-range prediction of european and north  
 364 american winters. *Geophysical Research Letters*, *41*(7), 2514–2519. doi:  
 365 10.1002/2014GL059637
- 366 Scaife, A., Karpechko, A. Y., Baldwin, M., Brookshaw, A., Butler, A., Eade, R., ...  
 367 others (2016). Seasonal winter forecasts and the stratosphere. *Atmospheric*  
 368 *Science Letters*, *17*(1), 51–56. doi: 10.1002/asl.598
- 369 Thompson, D. W., & Wallace, J. M. (1998). The arctic oscillation signature in  
 370 the wintertime geopotential height and temperature fields. *Geophysical Re-*  
 371 *search Letters*, *25*(9), 1297–1300. doi: 10.1175/1520-0442(2004)017%3C3990:  
 372 DCSOTN%3E2.0.CO;2
- 373 Thompson, D. W., & Wallace, J. M. (2001). Regional climate impacts of the north-  
 374 ern hemisphere annular mode. *Science*, *293*(5527), 85–89. doi: 10.1126/science  
 375 .1058958
- 376 Trascasa-Castro, P., Maycock, A. C., Scott Yiu, Y. Y., & Fletcher, J. K. (2019).  
 377 On the linearity of the stratospheric and euro-atlantic sector response to enso.  
 378 *Journal of Climate*, *32*(19), 6607–6626. doi: 10.1175/JCLI-D-18-0746.1
- 379 Wang, L., Ting, M., & Kushner, P. (2017). A robust empirical seasonal prediction  
 380 of winter nao and surface climate. *Scientific Reports*, *7*(1), 1–9. doi: 10.1038/  
 381 s41598-017-00353-y
- 382 Wang, W., Anderson, B. T., Kaufmann, R. K., & Myneni, R. B. (2004). The rela-  
 383 tion between the north atlantic oscillation and ssts in the north atlantic basin.  
 384 *Journal of Climate*, *17*(24), 4752–4759. doi: 10.1175/JCLI-3186.1
- 385 Wilks, D. (2019). *Statistical Methods in the Atmospheric Sciences*. Elsevier.
- 386 Wohltmann, I., von der Gathen, P., Lehmann, R., Maturilli, M., Deckelmann, H.,  
 387 Manney, G. L., ... Rex, M. (2020). Near complete local reduction of arc-  
 388 tic stratospheric ozone by severe chemical loss in spring 2020. *Geophysical*  
 389 *Research Letters*. doi: 10.1029/2020GL089547

# Supporting Information for “Seasonal Forecasts of the Exceptional Northern Hemisphere Winter of 2020”

Simon H. Lee<sup>1</sup>, Zachary D. Lawrence<sup>2,3</sup>, Amy H. Butler<sup>2,4</sup>, and Alexey Y.

Karpechko<sup>5</sup>

<sup>1</sup>Department of Meteorology, University of Reading, Reading, UK

<sup>2</sup>Cooperative Institute for Research in Environmental Sciences (CIRES), University of Colorado, Boulder, Colorado, USA

<sup>3</sup>NOAA Physical Sciences Laboratory (PSL), Boulder, Colorado, USA

<sup>4</sup>NOAA Chemical Sciences Laboratory (CSL), Boulder, Colorado, USA

<sup>5</sup>Finnish Meteorological Institute, Helsinki, Finland

## Contents of this file

1. Table S1
2. Figures S1 to S2

**Table S1.** Details of the 6 seasonal forecast models used in this study. In a “burst” ensemble the entire ensemble is produced at the same time, while “lagged” ensembles are produced as a collection of smaller ensembles over several days. The number in parentheses indicates the hindcast ensemble size. Accessed from <https://confluence.ecmwf.int//display/CKB/Description+of+the+C3S+seasonal+multi-system>.

<b>Center</b>	<b>Model</b>	<b>Ens. Type</b>	<b>Ens. Size (Hindcasts)</b>	<b>Resolution</b>
CMCC	CMCC-SPS3	Burst	50 (40)	1° lat-lon L46
DWD	GCFS 2.0	Burst	50 (30)	T127 L95
ECMWF	SEAS5	Burst	51 (25)	Tco319 L91
Météo-France	System 7	Lagged	51 (25)	TL359 L91
NCEP	CFSv2	Lagged	120 (24)	T128 L64
UKMO	GloSea5-GC2	Lagged	60 (28)	N216 L85

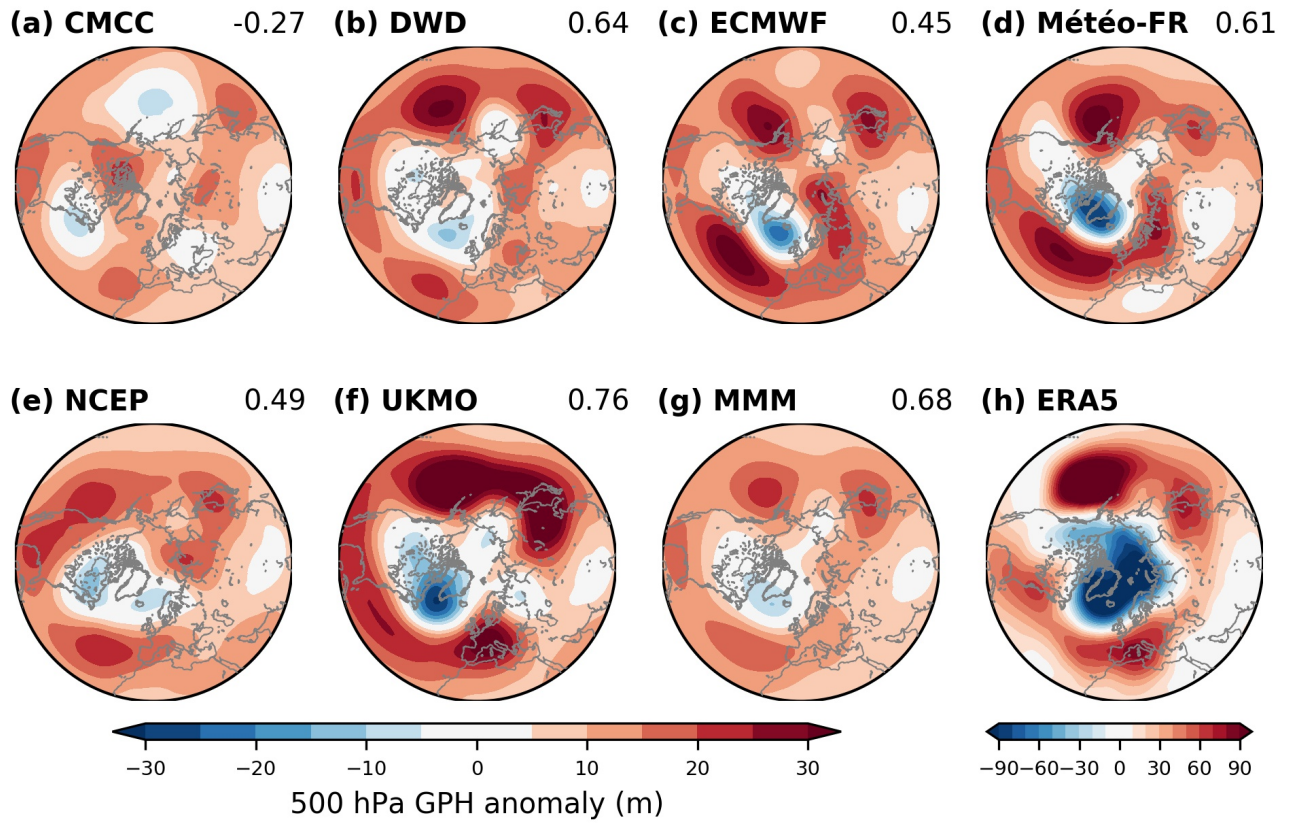


**Figure S1.** As Figure 1 (a–h) in the main text, but for forecasts nominally initialized on 1 October 2019.

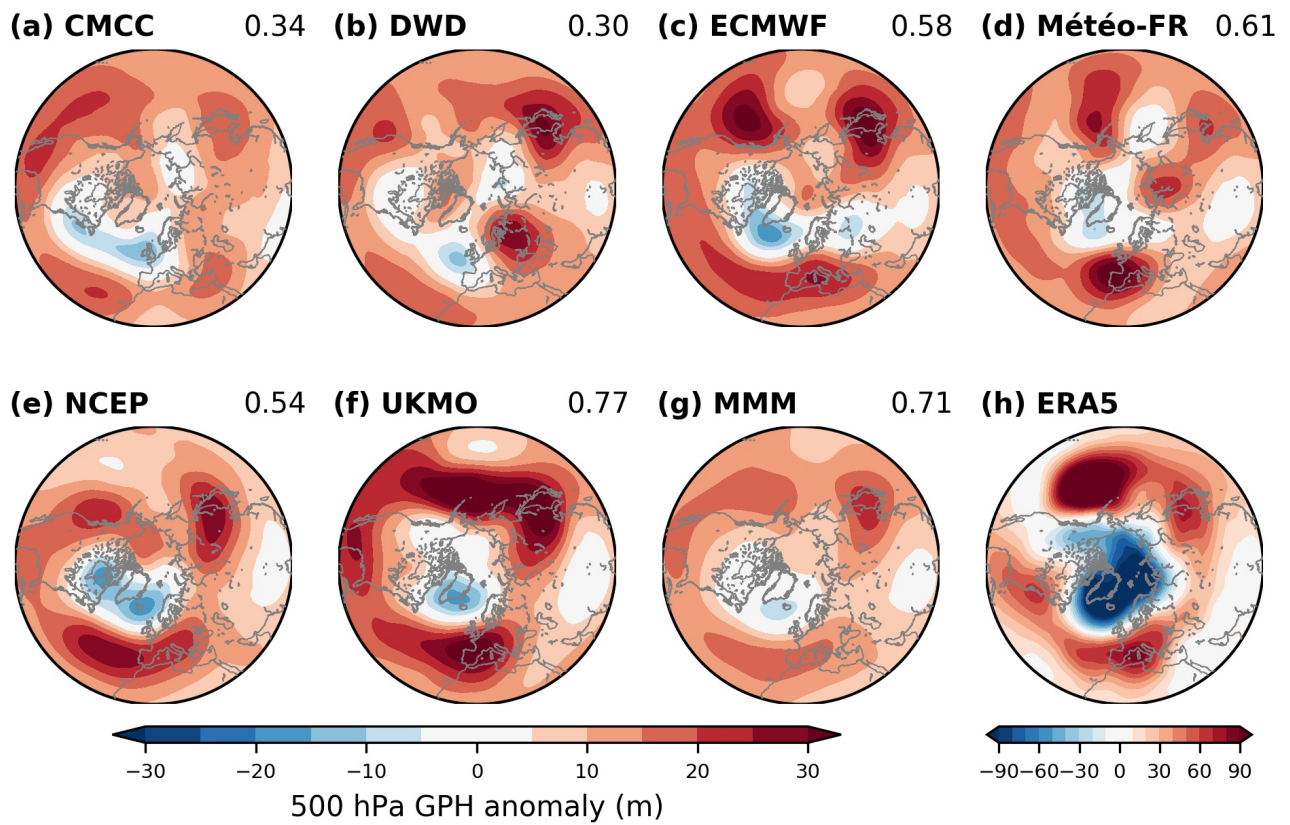


**Figure S2.** As Figure S1 but for forecasts nominally initialized on 1 November 2019.